iJET EXPLORE International Journal of Engineering & Technology
CENTRE OF PROFESSIONAL RESEARCH PUBLICATIONS
ISSN 2049-3444

International Journal of Engineering and Technology Volume 3 No. 6, June, 2013

Design and Characterisation of a Piezoelectric Bimorph Energy Harvesting Device

Action Nechibvute[1*], Albert Chawanda[1], Pearson Luhanga [2]
[1]Physics Department, Midlands State University, P/Bag 9055, Gweru, Zimbabwe
[2]Physics Department, University of Botswana, P/Bag 0022, Gaborone, Botswana

ABSTRACT

The power output of piezoelectric energy harvesting devices can be improved by optimizing the geometry of the device. In this paper, we present our design and experimental results on the electrical power output of a vibration based piezoelectric bimorph device with a proof mass. A geometrical optimization procedure was implemented and the results suggest that the series bimorph device is optimized for power generation when the ratio of the piezoelectric layer length to the proof mass length is 50 %. The optimized device with a volume of 0.678 cm^3 was fabricated and its performance was experimentally evaluated. The studies demonstrated that the device was capable of delivering a maximum of 344.67 μW of power to a matched resistive load of 230.6 kΩ, when driven by an ambient mechanical acceleration of 0.45 g at the resonance frequency of 51.5 Hz. This represents a power density of 508 $\mu W/cm^3$, which is over five times the nominal power density of 100 $\mu W/cm^3$ required for powering a wireless sensor.

Keywords: *piezoelectric bimorph, optimum design, energy harvesting, characterisation*

1. INTRODUCTION

During the past decade, there has been an emerging interest in the design of wireless data transmission systems powered by energy harvesting devices [1-4]. Such systems have a wide range of applications including: wireless sensor networks used for structural health monitoring, self-powered embedded microsensors for industrial instrumentation and machine monitoring, battery-free implantable medical devices, and long term sensors used for environmental management [5,6]. The traditional way to power remote sensor systems and distributed low power network devices is to use batteries. However, the use of batteries has several limitations, including relatively large size as compared with the devices they power, finite amount of energy contained, limited shelf life, and possible hazard problem by chemical leakage. Harvesting energy from the environment is a potential alternative power source that can address the limitations presented by use of batteries in powering remote and off-grid micro-electronic devices. Mechanical vibrations are perhaps the most ubiquitous ambient source of energy that can be harvested. The three transduction mechanisms which can be used to get electrical energy from this source are electromagnetic, electrostatic or piezoelectric effects [1,2]. Compared with other transduction mechanisms, piezoelectric based energy harvesting has attracted significant interest because it can harvest energy over a wide range of frequencies and can be easily applied using simple electromechanical structures [1,7,8]. The main challenge in piezoelectric energy harvesting is that generally the power generated by piezoelectric devices is low compared to the power requirements of most electronic devices. While several researchers have addressed this challenge by introduction of novel power conditioning circuits [9, 10], the use of geometric optimization of device dimensions has been greatly neglected by researchers [11].

This paper is dedicated to proposing a new optimized geometric design for a piezoelectric bimorph energy harvesting device with a proof mass. The device was designed for applications in machine environments that resonate at the designated mains frequency of 50 Hz. The length of the piezoelectric layer and the length of the proof mass that optimized the power generated at a specified resonance frequency and device volume were studied using numerical analysis and the Finite Element Method (FEM) software package, COMSOL Multiphysics® (version 4.3). The device performance was evaluated by experiments.

2. MODELING AND OPTIMIZATION

2.1 FEM Study in COMSOL

The modeling of the cantilever beam with a proof mass was done using COMSOL Multiphysics® FEM software. COMSOL Multiphysics® is a powerful interactive environment for modeling and solving all kinds of scientific and engineering problems. The software provides a powerful integrated desktop environment with

a *Model Builder* where one gets full overview of the model and access to all functionality [12]. The COMSOL package is user friendly mainly due to the preset physics interfaces, which can be used to include the governing equations from a wide variety of physics problems into a model. A single model can include and couple several physics interfaces to allow for interactions that are often observed in the real world. Some of these coupled situations also exist as predefined physics interfaces. COMSOL Multiphysics® has been successfully used by other researchers in modeling and design of piezoelectric devices [13-16]. In this study, the piezoelectric devices interface (*pzd*), which is a combination of solid mechanics and electrostatics, is employed. The *pzd* interface solves the piezoelectric problem based on the standard piezoelectric constitutive equations.

The first study performed was the eigenfrequency analysis. In this study, the aim was to determine the geometrical parameters of the device that result in a first resonance frequency of 52 Hz. The built-in CAD tools were used to draw the geometry and domains governed by the appropriate physics interfaces were set. This was followed by assigning materials and geometrical parameters shown in Table 1 to the domains in the model.

The conditions to domains and boundaries were applied such that the piezoelectric layers are poled for series connection. The model was designed so that the device is clamped on one end leaving the rest of the cantilever to vibrate freely. This was achieved by applying a fixed constraint on the vertical side of the device along the width. The model was then submitted for meshing using the standard meshing tool for extra fine elements. In this simulation study, a minimum of 2973 quadrilateral elements with average element quality of 0.8333 was used. Fig. 1 shows the 3D and 2D meshed geometry used for the design study.

The 2D meshed geometry was submitted for the eigenfrequency study. Fig. 2 shows the first three resonance modes of the device. Using the procedure outlined above, the geometric parameters of the design were manually adjusted until the first resonance frequency (f_r) of the device was 52 Hz. Table 2 shows the results of this study.

D1 to D8 denote the different device designs. Note that the total device length was kept at 27 mm and the width was fixed at 4 mm. The width of the beam was the same as the width of the proof mass. The parameter β denotes the ratio of the piezoelectric layer to the length of the proof mass.

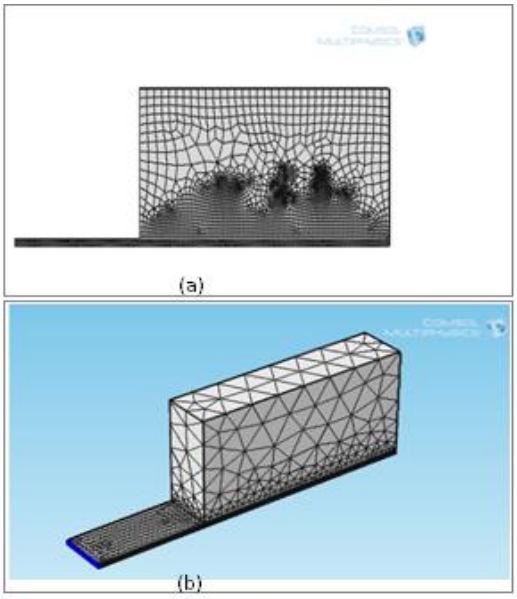

Fig. 1: Meshed geometry in COMSOL (a) 2D and (b) 3D

Table 1: Material Properties and Geometric Parameters

Substrate : stainless Steel	
Young Modulus (GPa)	200
Poisson ratio	0.30
Density ρ_s (kgm^{-3})	7800
Length x width x thickness (mm)	27 × 4.0 × 0.120
Piezoelectric material: PSI-5H4E (Piezo Systems Inc, MA)	
Young's modulus (GPa)	
E_{11}	62
E_{33}	50
Poission's ratio	0.3
Elastic constants:(GPa)	
C_{11}	110.8
C_{12}	49.8
C_{13}	49.8
C_{33}	110.8
C_{44}	30.5
Density ρ_p(kg/m3)	7800
Piezoelectric constants (×10^{-12} m/volt)	
d_{33}	650
d_{31}	-320
Coupling coefficients	
k_{33}	0.75
k_{31}	0.44
Relative dielectric constant ε_{33}	3800
Mechanical quality factor Q	32
*Length×width×thickness (mm)	*L_b × 4.0 × 0.127
Proof mass material: lead	
Young's modulus (GPa)	14
Poisson's ratio μ_s	0.42
Density ρ_m (kg/m^3)	11340
*Length×width×*height (mm)	*L_m × 4.0 × *h_m

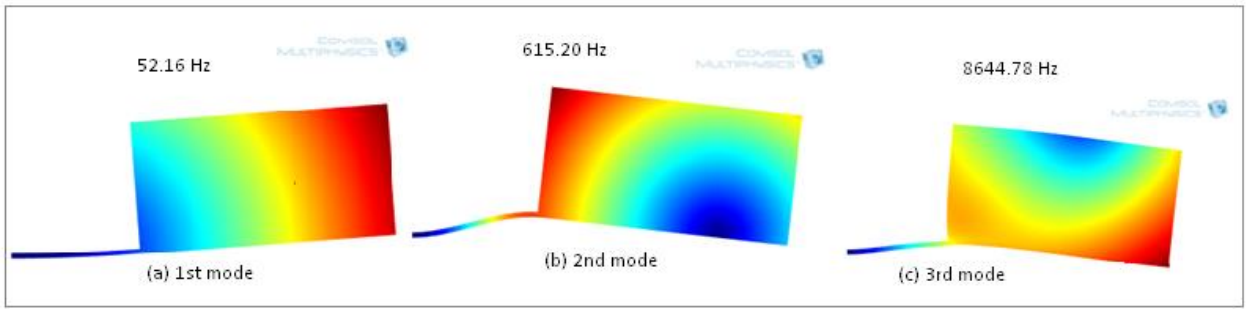

Fig. 2: First three resonance modes

Table 2: Different geometries that give a targeted resonance frequency of ~ 52 Hz

Device Geometry	Piezoelectric layer length L_b (mm)	Proof mass length L_m (mm)	Proof mass height h_m (mm)	$\beta = \frac{L_b}{L_m}$ [%]	Device volume (cm^3)	Capacitance C_p (nF)	f_r (Hz)
D_1	5.0	22.0	11.45	22.73	1.048	2.649	52.1831
D_2	6.0	21.0	10.50	28.57	0.922	3.179	52.1359
D_3	7.0	20.0	9.80	35.00	0.824	3.709	52.1170
D_4	9.0	18.0	8.88	50.00	0.678	4.769	52.1600
D_5	10.0	17.0	8.60	58.82	0.625	5.298	52.1627
D_6	11.0	16.0	8.45	68.75	0.581	5.828	52.0466
D_7	12.0	15.0	8.30	80.00	0.539	6.358	52.1294
D_8	13.0	14.0	8.25	92.86	0.502	6.888	52.1327

2.2 Optimization of Design

The device geometries from D1 to D8 shown in Table 2 are all resonant when operating at 52 Hz. The key question to be addressed in this section is:

which of the devices represent the best design in the context of power output?

A typically good design will result in a device with low capacitance and low device volume. However, these are conflicting and hence difficult to trade off since a low capacitance device tends to be the device with the largest volume (see Table 2). On the other hand the device with the lowest volume is the very device with the highest capacitance! Thus there is need to introduce an additional parameter that will give a reasonable device volume while dictating the minimum possible capacitance for the device. We have chosen the electromechanical coupling parameter (θ) as the most appropriate parameter. For an energy harvesting device operating at resonance frequency ω, the peak voltage (V) delivered to the resistive load (R) is given by Eq. (1) [17]:

$$V = \frac{m\omega^2\theta B_m u_0}{c\left(j\omega C_p + \frac{1}{R}\right) + \theta^2} \quad (1)$$

where the m is the equivalent mass, B_m is the base excitation-forcing term, u_0 is the translational excitation amplitude, c is the damping parameter given by $c = 2\xi\omega m$, ξ is the damping ratio, and $j = \sqrt{-1}$.

The average power (P) in terms of the peak voltage delivered to the resistive load is given by Eq. (2):

$$P = \frac{|V|^2}{2R} \quad (2)$$

For a given beam design geometry, specified resistive load and excitation frequency, the output voltage as defined by Eq. (1) and hence the power harvested given by Eq. (2), is a function of the coupling parameter (θ) and the piezoelectric capacitance of the bimorph (C_p). The electromechanical coupling parameter needs to be maximized while the capacitance needs to be minimized [17]. For a given value of resistive load and the damping ratio, the value of the coupling parameter that maximizes the power is such that $\theta^2 = c/R$.

For the typical case where ξ = 1 % and R = 250 kΩ, the values of θ that optimizes the power were calculated for the different design geometries shown in Table 2. The value of θ was normalized such that it is unit for the piezoelectric coverage length (L_b) closest to the clamped end (i.e. the root of the cantilever). Fig. 3 shows the results of this numerical study.

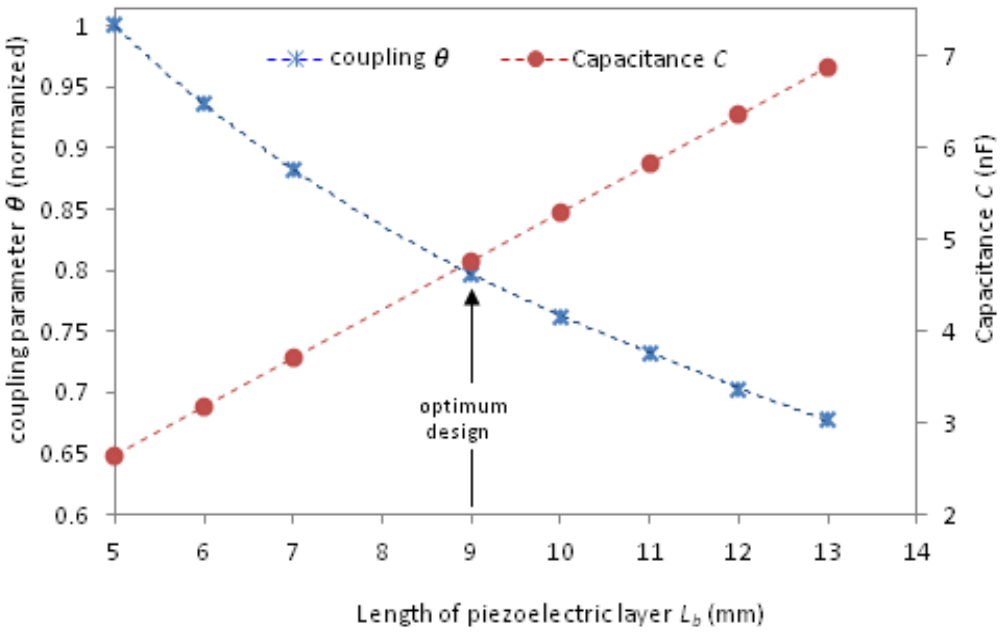

Fig. 3: Plot of coupling parameter and capacitance as a function of piezoelectric length

Fig. 3 shows that a piezoelectric length of 9 mm corresponding to β = 50 % gives the maximum voltage and hence the maximum power. Compared to all the possible device geometries in Table 2, design D4 represents optimized device geometry. As a simple way of performing a sensitivity analysis, the design geometries within the vicinity of D4 where subjected to a stationary study in COMSOL, with a boundary load (F_{tot}) at the tip of the proof mass. The results of the generated electric potential confirm that D4 is the optimum design since it yields the largest electric potential for the three values of the applied tip load F_{tot} (see Table 2)

Table 2: Sensitivity Analysis results using COMSOL

	Electric potential (V)		
Static tip Load F_{tot} (N)	D3	D4 (optimized)	D5
0.01	3.1483	3.1485	3.1484
0.02	6.2966	6.297	6.2968
0.03	9.4449	9.4455	9.4453

The next task was to fabricate and experimentally evaluate the performance of the device realized using design D4.

3. EXPERIMENTAL PROCEDURES

The optimized geometry D4 with dimensions shown in Table 2 was fabricated. The device is principally a sandwich structure with a central stainless steel substrate and two piezoelectric material layers (PSI-5H4E, Piezo Systems Inc. ,USA); one bonded to the top and the other to the bottom of the central stainless steel layer. A lead proof mass was attached to the substrate beam using Super Glue to tune the frequency of the beam device to a targeted resonance frequency. Note that the nickel electrode on the piezoelectric layer was removed using a fine sand paper for the parts that lie underneath the proof mass to reduce device capacitance [18,19]. The device was fastened to an aluminium fixture on an electromagnetic shaker using screws. The shaker was driven by signal from the function generator and dual amplifier to supply a sinusoidal force of desired magnitude and frequency. The acceleration level was measured using the ADXL202 accelerometer (Analogue Devices, USA), which has a typical sensitivity of 312 mV/g when operating from a 5 V power supply.

Fig. 4 shows a snapshot image of the optimized device. The accelerator output signal and the output voltage signal from the device were monitored by a digital storage oscilloscope (ISOTECH-IDS-8062). A variable resistor box was connected across the output terminals of the device to enable the measurements of voltage and power output for different resistive load values (from 47 kΩ to 840 kΩ in steps of 47 kΩ). With the excitation signal set at an acceleration of 0.45 g and the frequency set at resonance (i.e. f_r = 51.5 Hz), the voltage and power values delivered to different load resistances was measured. The procedure was repeated for difference excitation frequencies so as to determine the off-resonance performance of the device. The results are presented in the next section.

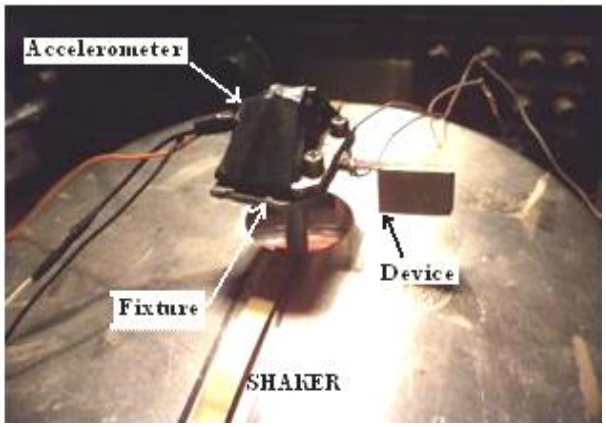

Fig. 4: Device Clamped on Shaker

4. EXPERIMENTAL RESULTS

The first test performed was the experimental determination of the resonance frequency by measuring the output voltages from different excitation frequencies. As shown in Fig. 5 the experimental value of the resonance is 51.5 Hz. The results of power and voltage measurements are shown in Figs. 6 and 7 respectively.

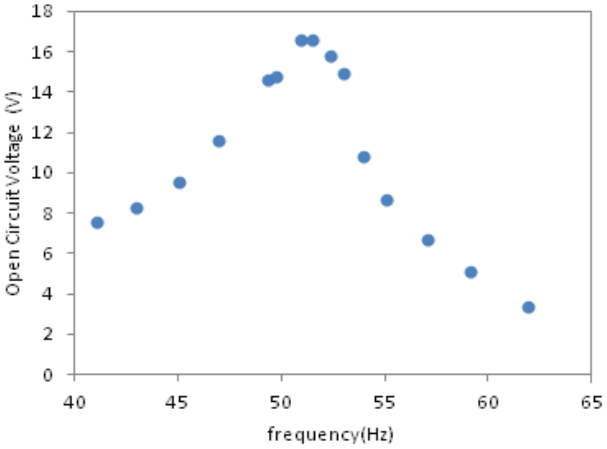

Fig. 5: variation of open circuit voltage with frequency

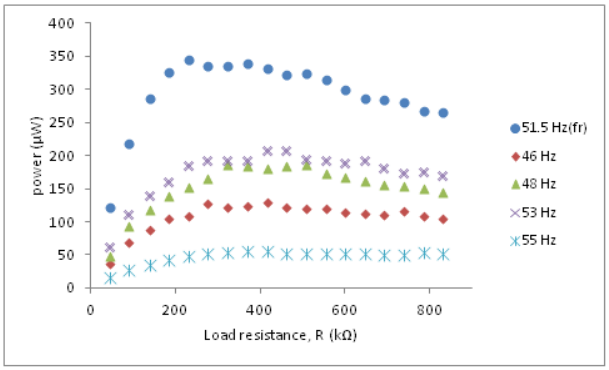

Fig. 6: variation of output power with resistive load for various excitation frequencies

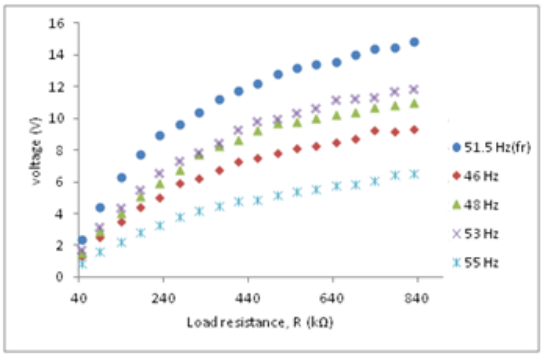

Fig. 7 variation of output voltage with resistive load for various excitation frequencies

5. DISCUSSION

The value of the first resonance frequency obtained by experiment compares very well with the simulation result of 52.16 Hz (an overestimation by only 0.6 %) obtained using eigenfrequency analysis in COMSOL. The FEM software enables a convenient and fast way of determining the resonance nodes while at the same time giving a visual picture of the appearance of the modes. The effect of geometrical parameter variations of a particular design could be studied in a faster way compared to the standard analytical approaches.

The result of the optimization study show that the device is optimized for power generation when the ratio of the piezoelectric layer length to the proof mass length is 50 % . This corresponds to a piezoelectric coverage of 1/3 of the total beam length. Contrary to the common practice of covering the entire beam with piezoelectric layer [1-3,6-8], the result shows that a piezoelectric coverage of 1/3 optimized the power generated. Any coverage above this value will lead to an increased capacitance and a reduced electromechanical coupling. Energy losses due to charge re-distribution will significantly reduce the voltage and power output of the device for large capacitances [20].

The results in Fig. 6 show that output voltage increases with increasing resistive load and that the voltage then becomes saturated upon further resistive loading. The highest voltage is obtained at resonance, with a drift from resonance of about 2 Hz resulting in a voltage loss of around 2 V. Fig. 7 shows that a maximum power of 344.67 μW at 8.92 Vrms into an optimum resistance of 230.6 kΩ was generated at a resonance frequency of 51.5 Hz. The experimental results also demonstrate that the device is able to deliver at least a power density of 100μW/cm^3 for the operating frequencies from 46 Hz to 53 Hz. The energy harvesting power density is an important figure of merit which is used to quantify the performance of energy harvesting devices and is defined as the power output divided by the device volume. At

resonance, the device in this study delivered 344.67 μW to a matched load. Since the device has a volume of 0.678 cm^3, the power density is 508 $\mu W/cm^3$. This is a very high power density compared to the average value of 100 $\mu W/cm^3$ typically required to power a wireless sensor [1,2,6,8]. The optimized device has a power output which is comparable to those presented in [3, 18, 19] in which the power output reported were 365 μW [3], 335 μW [18], and 370 μW [19] for a device volume of 1 cm^3 under an excitation acceleration of 0.23 g.

Future studies will consider designing tuning techniques to increase the operating frequency range and hence widening the bandwidth of the energy harvesting device. Application of synchronous switching techniques will further enhance the power output of the device under off resonance conditions.

6. CONCLUSION

The optimization study showed that a piezoelectric to proof mass length ratio of 50 % optimized the power generated by a piezoelectric energy harvesting device. The fabricated optimized prototype device was experimentally characterized and shows that a maximum power density of 508 $\mu W/cm^3$ could be delivered to a matched resistive load at resonance and under 0.45 g acceleration. While this device would generate enough power to power a typical sensor node, the operation frequency of the device is narrow. As further research, there is need to investigate techniques that could be employed to broaden the working frequency of the energy harvester.

ACKNOWLEDGEMENT

The authors would like to thank the Midlands State University Research Board for funding this research.

REFERENCES

[1] S. Roundy, P.W. Wright, and J. Rabaey, "A study of low level vibrations as a power source for wireless sensor nodes," *Comput. Commun.*, vol. 26, pp.1131-1144, 2003.

[2] S. P. Beeby, M. J. Tudor, and N. M. White, "Energy harvesting vibration sources for microsystems applications," *Meas. Sci. Technol.*, vol. 17, no. 12, pp. R175–R195, 2006.

[3] P. D. Mitchson, E. M. Yeatman, G. K. Rao, A. S. Holmes, and T. C. Green, "Energy harvesting from human and machine motion for wireless electronic devcies," *Proc. IEEE*, vol. 96, no. 9, pp. 1457–1486, Sep. 2008.

[4] C.-Y. Chong and S. P. Kumar, "Sensor Networks: Evolution, Opportunities, and Challenges," *Proceedings of the IEEE*, vol. 91, no. 8, pp. 1247–1256, August 2003.

[5] W. K. G. Seah, Z. A. Eu, and H.-P. Tan, "Wireless Sensor Networks Powered by Ambient Energy Harvesting (WSN-HEAP) – Survey and Challenges," Invited paper, in *Proceedings of the First International Conference on Wireless Communications, Vehicular Technology, Information Theory and Aerospace & Electronic Systems Technology (Wireless VITAE)*, Aalborg, Denmark, 17-20 May 2009.

[6] R. Vullers, R. Schaijk, H. Visser, J. Penders, and C. Hoof, "Energy Harvesting for Autonomous Wireless Sensor Networks," *IEEE Solid-State Circuits Magazine*, vol. 2, no. 2, pp. 29–38, Spring 2010.

[7] Y . C. Shu and I. C. Lien, "Analysis of power output for piezoelectric energy harvesting systems," *Smart Mater. Struct.*, vol. 15, pp. 1499–1512, 2006.

[8] S . Roundy, E. S. Leland, J. Baker, E. Carleton, E. Reilly, E. Lai, B.Otis, J. M. Rabaey, P. K. Wright, and V. Sundararajan, "Improving power output for vibration-based energy scavengers," *IEEE Trans. Pervasive Comput.*, vol. 4, pp. 28–36, 2005.

[9] G. K. Ottman, H. F. Hofmann, and G. A. Lesieutre, "Optimized piezoelectric energy harvesting circuit using step-down converter in discontinuous conduction mode," *IEEE Trans. Power Electron.*, vol.18, pp. 696–703, 2003.

[10] D. Guyomar and M. Lallart, "Recent Progress in Piezoelectric Conversion and Energy Harvesting Using Nonlinear Electronic Interfaces and Issues in Small Scale Implementation," *Micromachines*, vol.2, pp. 274-294, 2011.

[11] M. W. Shafer, M. Bryant and E. Garcia, "Designing maximum power output into piezoelectric energy harvesters," *Smart Mater. Struct.*, vol. 21, no. 8, p. 085008, 2012.

[12] COMSOL, "COMSOL Multiphysics 4.3 Documentation", www.comsol.com, 2012.

[13] M. D. Salim, H. Salleh, and D.S.M. Salim, "Simulation and experimental investigation of a wide band PZ MEMS harvester at low frequencies," *Microsyst. Technol.*, vol. 18, pp. 753–763, 2012.

[14] S. N. Jagtap and R. Paily, "Geometry Optimization of a MEMS-based Energy Harvesting Device,"

Proceeding of the IEEE Students' Technology Symposium (TechSym), IIT Kharagpur, pp. 265 – 69, 2011.

[15] V. Rajendran, P. Sukumar and L. Sujatha, "Modeling and simulation of MEMS energy harvester," *Telecommunications Energy Conference (INTELEC), IEEE 33rd International*, Amsterdam, 9-13 Oct. 2011.

[16] V. Piefort, "Finite Element Modelling of Piezoelectric Active Structures," PhD Dissertation, Universiteé Libre de Bruxelles. Belgium, 2001.

[17] M. I. Friswell and S. Adhikari, "Sensor shape design for piezoelectric cantilever beams to harvest vibration energy," *J. Appl. Phys*., vol. 108, no. 1, p. 014901, 2010.

[18] S. Roundy, P. K. Wright and J. M. Rabaey, Energy Scavenging for Wireless Sensor Networks: With Special Focus on Vibrations. Springer, 2004.

[19] M. Zhu and E. Worthington, "Design and Testing of Piezoelectric Energy Harvesting Devices for Generation of Higher Electric Power for Wireless Sensor Networks," *Proceedings of the IEEE Sensors*, Christchurch, New Zealand, pp. 699 – 702, 2009.

[20] M. Stewart, P. M. Weaver and M. Cain, "Charge redistribution in piezoelectric energy harvesters," *Appl. Phys. Lett.*, vol. no. 7, p. 073901, 2012.